Environmental Science & Technology

Article

pubs.acs.org/est

Eutrophication-Driven Hypoxia in the East China Sea off the Changjiang Estuary

Hongjie Wang,[†,‡] Minhan Dai,[*,†] Jinwen Liu,[†] Shuh-Ji Kao,[†] Chao Zhang,[†] Wei-Jun Cai,[§] Guizhi Wang,[†] Wei Qian,[†] Meixun Zhao,[∥] and Zhenyu Sun[†]

[†]State Key Laboratory of Marine Environmental Science, Xiamen University, Xiamen 361102, China

[‡]Department of Physical & Environmental Sciences, Texas A & M University-Corpus Christi, Corpus Christi, Texas 78412, United States

[§]School of Marine Science and Policy, College of Earth, Ocean, & Environment, University of Delaware, Newark, Delaware 19716, United States

[∥]Key Laboratory of Marine Chemistry Theory and Technology, Ocean University of China, Qingdao, China

ABSTRACT: Coastal hypoxia is an increasingly recognized environmental issue of global concern to both the scientific community and the general public. We assessed the relative contributions from marine and terrestrially sourced organic matter that were responsible for oxygen consumption in a well-studied seasonal coastal hypoxic zone, the East China Sea off the Changjiang Estuary. Our fieldwork was conducted in August 2011 during reinstatement of a subsurface hypoxia, when we observed a continuous decline of dissolved oxygen along with production of dissolved inorganic carbon resulting from organic carbon remineralization. On the basis of a three end-member mixing model and determinations of the stable isotopic compositions of dissolved inorganic carbon ($\delta^{13}C_{DIC}$), the end product of particulate organic carbon (POC) degradation, we quantified the $\delta^{13}C$ value of the remineralized organic carbon ($\delta^{13}C_{OCx}$), which was −18.5 ± 1.0‰. This isotopic composition was very similar to the $\delta^{13}C$ of marine sourced POC produced *in situ* (−18.5 ± 0.3‰) rather than that of the terrestrially sourced POC (−24.4 ± 0.2‰). We concluded that marine-sourced organic matter, formed by eutrophication-induced marine primary production, was the dominant oxygen consumer in the subsurface hypoxic zone in the East China Sea off the Changjiang Estuary.

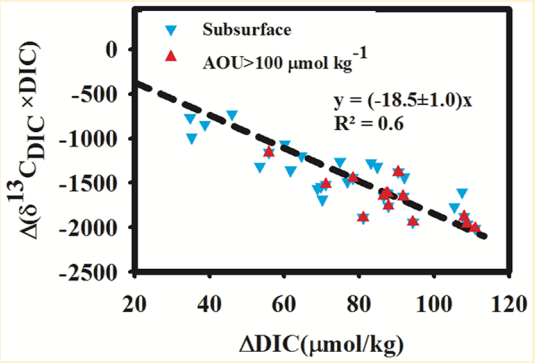

1. INTRODUCTION

Hypoxia, where dissolved oxygen (DO) concentrations are less than 2 mg L^{-1} (or 62.5 μmol L^{-1}), is reported to be spreading at a dramatically increasing rate in the coastal oceans of the world and receives wide attention from both the scientific community and the general public.[1−3] Hypoxia could deteriorate ecosystem services such as biodiversity and fisheries,[3−5] alter biogeochemical cycles of elements,[6] and increase the susceptibility of coastal waters to ocean acidification.[7]

It is generally agreed that the formation of coastal hypoxia results from an imbalance between oxygen supply and consumption in a stratified water column. In warm and wet seasons, the formation of vertical stratification in the water column as a consequence of surface heating and/or freshwater outflow inhibits oxygen penetration from the surface into the subsurface. In this hydrologically confined subsurface regime, oxygen is consumed while organic material is remineralized. When the oxygen consumption exceeds its supply through advective and vertical mixing for an extensive period, hypoxia is formed.[2,3,5,8]

Many studies have suggested that hypoxia is primarily associated with marine-sourced organic carbon (OC_{mar}) production, which is stimulated by coastal eutrophication resulting from excessive terrestrial nutrient runoff.[5,9−12] Excess nutrients are believed to stimulate phytoplankton blooms in the surface waters, and sinking and remineralization of the algal biomass would contribute to DO consumption below the pycnocline. Therefore, oxidation of OC_{mar} is believed to be the predominant oxygen sink.[13−17] However, it is also reported that terrestrial OC (OC_{terr}), typically transported by river runoff and coastal erosion, may also play a significant role in the development of hypoxia.[18−20] For example, Dagg et al.[21] suggest that OC_{mar} can support only 23% of the DO consumption in the Gulf of Mexico hypoxic zone, and thus, OC_{terr} may also play an important role in the formation of hypoxia.[18,20,22]

Resolving this controversy requires a mechanistic and quantitative approach to determine the relative contributions of marine versus terrestrially sourced OC (i.e., OC_{mar} vs OC_{terr}) in consuming DO. This information is vitally important for

Received: December 19, 2015
Revised: January 29, 2016
Accepted: January 29, 2016
Published: January 29, 2016

DOI: 10.1021/acs.est.5b06211
Environ. Sci. Technol. 2016, 50, 2255−2263

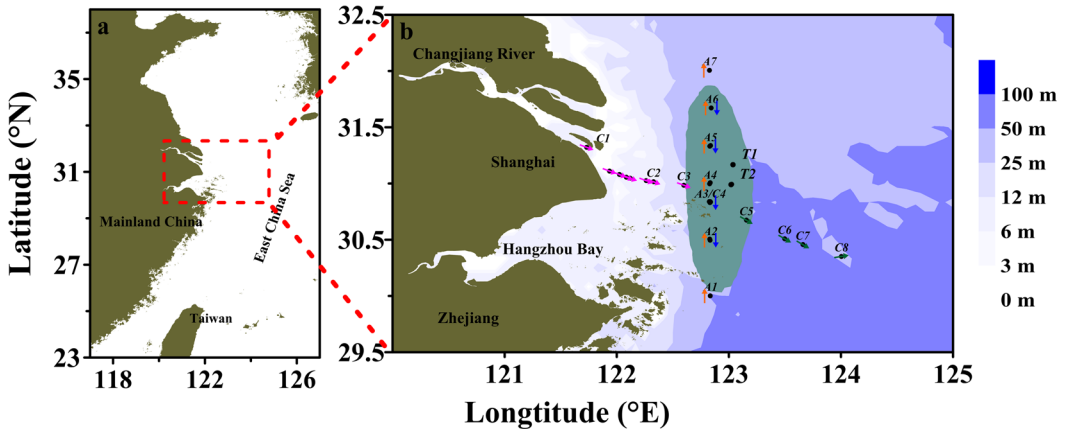

Figure 1. Study area (red box) in the East China Sea (a) and sampling sites in the outer Changjiang Estuary in August 2011 (b). Isobaths are shown by blue shading. The shaded area in dark green represents the main hypoxic region at the bottom with dissolved oxygen content less than 2 mg L^{-1} (or 63 μmol L^{-1}) frequently reported in previous studies.

nutrient management and policy making in mitigating hypoxic conditions.[11,23,24]

We chose a well-known seasonal hypoxic zone in the East China Sea (ECS) off the Changjiang Estuary to examine the origins of the organic materials that consumed DO. Prior studies infer that both OC_{mar} and OC_{terr} may contribute to hypoxia formation,[8,10,17,25] although most researchers believe that terrigenous organic matter delivered by the Changjiang is not reactive enough to generate hypoxia.[26] However, studies to decipher the relative contribution of OC_{mar} and OC_{terr} in consuming DO are still lacking.[27] Our study was undertaken therefore to determine the concentration and isotopic compositions of both the particulate OC (POC) that is responsible for oxygen consumption and the end product of its oxidation, dissolved inorganic carbon (DIC). With the aid of three end-member water mass mixing and isotopic balance models, we discerned the relative contributions of OC_{mar} and OC_{terr} in consuming DO in the bottom water.

2. MATERIALS AND METHODS

2.1. Study Area. The Changjiang, or Yangtze River, is the third longest river in the world, with a drainage area of 1.8×10^6 km^2, and it contributes 9×10^{11} m^3 of freshwater to the ocean annually, ranking it fifth in the world. It is the world's fourth largest river in terms of sediment discharge.[28] This river is also highly anthropogenically impacted, carrying a large amount of terrestrial materials, including nutrients and OC from the drainage basins, into the ECS. These material fluxes are reported to be 8.64×10^{11} g yr^{-1} for NO_3^-, 2.39×10^{10} g yr^{-1} for PO_4^{3-}, 1.58×10^{12} g yr^{-1} for dissolved OC (DOC), and 1.52×10^{12} g yr^{-1} for POC.[29,30] Most significantly, the Changjiang has suffered from eutrophication for the past few decades. For example, the NO_3^- concentration at the river mouth increased about 4-fold in the past 40−50 years, that is, from 20.5 in the 1960s up to 59.1 in the 1980s and to 80.6 μmol L^{-1} in 2004.[31] Such an increase is attributed to the intensification of agriculture and the use of mineral fertilizers.[32,33]

The bottom hypoxia off the Changjiang estuary is controlled by freshwater discharge, primary production, water column stratification, bottom topography, and variations of the northward extension of the Taiwan Warm Current toward the estuary.[10,25,27,34,35] Typically, hypoxia begins to develop in late spring and early summer when stratification starts to form. It reaches its maximum in August, when phytoplankton blooms commonly occur in the Changjiang plume (CJP) at this particular region.[27,36] Hypoxia is alleviated in fall and finally disappears in winter.[27]

2.2. Sampling and Analysis. We sampled the ECS off the Changjiang Estuary (Figure 1) on board the R/V *Runjiang I* on August 15−24, 2011, 10 days after the passage of Typhoon Muifa (http://www.cwb.gov.tw) through the study area. Stations T1 and T2 were located near the center of a trough in the ECS where hypoxia is frequently reported.[10,17,25,34] Sampling was conducted twice along Transect A during August 15−16 and August 22−23 and four times at Station C4 on August 15, 19, 22, and 24 (Figure 1b). Our cruise covered a 10 day hypoxia reinstatement process after the typhoon perturbation and therefore provided a unique opportunity to pinpoint the sources of organic materials that were responsible for the formation of hypoxia.

According to the gauge record at the Datong Station, located 624 km to the west of the Changjiang Estuary mouth, water discharge peaked from June to August. The maximum was 45,500 m^3 s^{-1} on June 28. Typhoon Muifa was not strong enough to induce an unusually high water discharge, and there was only a small discharge peak after our cruise time.[37] During the investigation period, the varying magnitude of water discharge from the watershed was basically consistent with the pattern of the long-term mean,[38,39] suggesting that the present study represented a typical summer condition of the area in terms of terrestrial material discharge.[37]

Temperature and salinity profiles were obtained using a Sea-Bird 911 plus CTD with a precision of ±0.005 °C and ±0.005, respectively. Discrete samples were collected from GoFlo bottles. DO was measured using the traditional Winkler titration method with a precision of ±0.06 mg kg^{-1}.[40] DIC samples were measured using infrared detection following acid extraction of a 0.5 mL sample.[41] Ca^{2+} concentration was determined in the onshore laboratory using EGTA titration with a Metrohm 809 TITRANDO potentiometer, which had a precision better than ±5 μmol kg^{-1}.[42] Chl-*a* was measured using fluorometry following 90% acetone extraction, and the analytical error was ±1%.[43]

The $\delta^{13}C_{DIC}$ was determined directly from the headspace after acidification with H_3PO_4 on a Thermo Fisher Finnigan Delta V isotope ratio mass spectrometer (IRMS) with a Gas Bench II preparation module for trace gas samples in the Third Institute of Oceanography, State Oceanic Administration, China. The analytical precision was ±0.1‰ (n = 8). The standards we

DOI: 10.1021/acs.est.5b06211
Environ. Sci. Technol. 2016, 50, 2255−2263

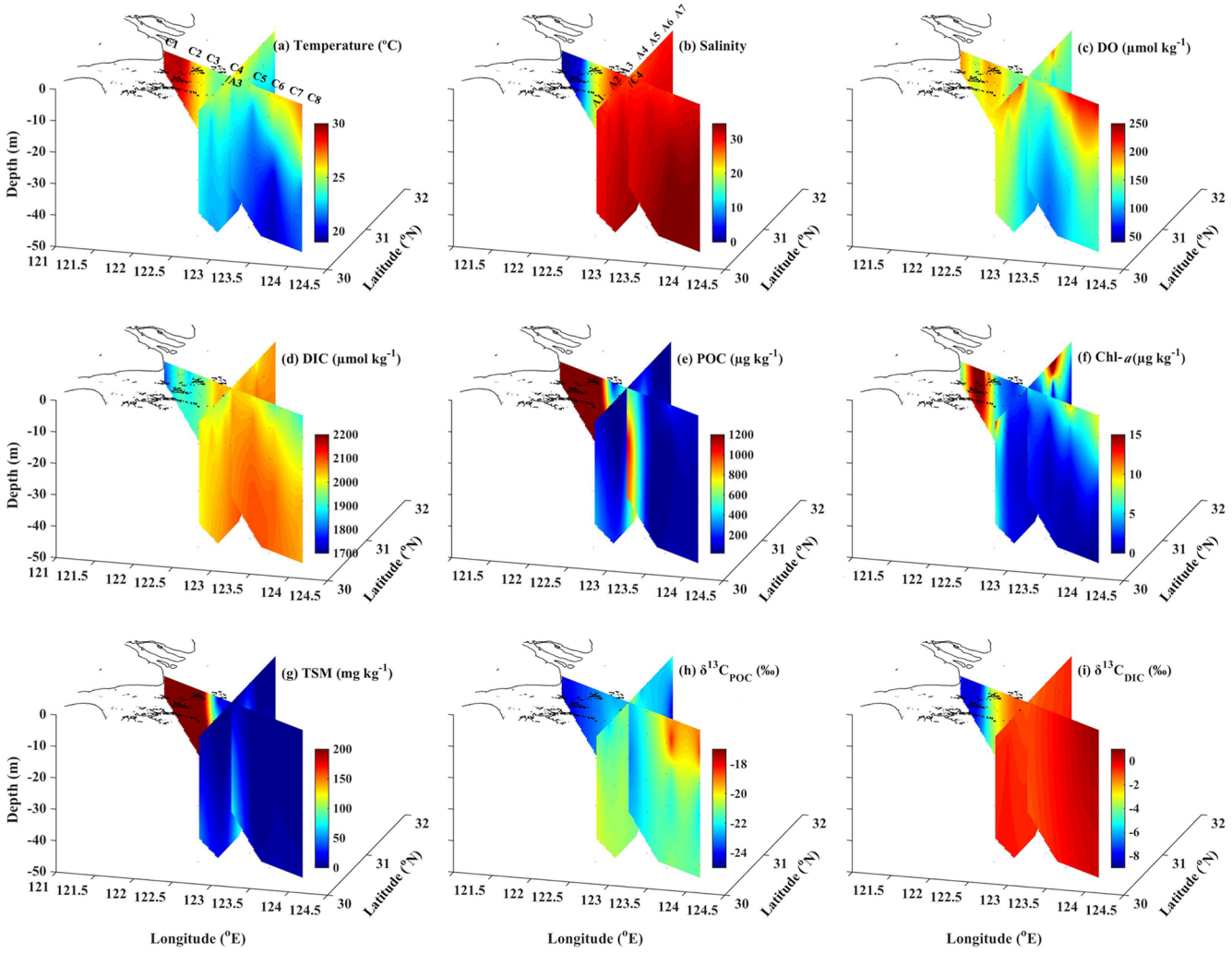

Figure 2. Distributions of (a) temperature, (b) salinity, (c) DO, (d) DIC, (e) POC, (f) Chl-*a*, (g) TSM, (h) $\delta^{13}C_{POC}$, and (i) $\delta^{13}C_{DIC}$ along Transects A and C. Note that the temperature, salinity, DO, Chl-*a*, and TSM data presented in panels (a), (b), (f), and (i) are reported elsewhere.[37,46]

used were IAEA-CO-1 ($\delta^{13}C = +2.492‰_{VPDB}$) and IAEA-CO-8 ($\delta^{13}C = -5.764‰_{VPDB}$).

Water samples for total suspended material (TSM), POC and $\delta^{13}C_{POC}$, were concentrated onto preweighted 47 mm Whatman GF/F membranes (nominated pore size: 0.7 μm, precombusted under 500 °C for 5 h) after filtering 0.5−4 L seawater under mild vacuum. TSM was obtained using the net weight increment on the membrane and the filtration volume. The membranes were then acidified with 1 mol L^{-1} HCl (guaranteed reagent) to remove carbonate minerals.[44] The decarbonated membrane was analyzed for POC and $\delta^{13}C_{POC}$ on an elemental analyzer coupled IRMS in the Key Laboratory of Marine Chemistry Theory and Technology, Ocean University of China. The analytical precision was ±0.1‰ ($n = 8$).[44,45] The standard used was IAEA−USGS-40 ($\delta^{13}C = -26.389‰_{VPDB}$). Note that part of the CTD, DO, TSM, and Chl-*a* data are applied as background hydrography in our parallel studies.[37,46]

2.3. Three End-Member Mixing Model. We utilized a three end-member mixing model based on mass conservation of potential temperature and salinity to predict conservative concentrations of a chemical of interest.[47,48]

$$f_1 + f_2 + f_3 = 1 \quad (1)$$

$$\theta_1 \times f_1 + \theta_2 \times f_2 + \theta_3 \times f_3 = \theta \quad (2)$$

$$S_1 \times f_1 + S_2 \times f_2 + S_3 \times f_3 = S \quad (3)$$

where θ and S represent potential temperature and salinity, and f_1, f_2, and f_3 denote the fractional contribution from three end-members. Here in this paper, we applied the model to the study area to predict DIC and its isotopic composition ($\delta^{13}C_{DIC}$) solely from conservative mixing. The offset between field values and model-predicted values represented the biologically altered fractions (Δ).

3. RESULTS

The distribution of the major parameters along Transects A and C surveyed on August 15−24, 2011, off the Changjiang Estuary is shown in Figure 2. The variability alongshore on Transect A was much less than that across-shelf on Transect C. The latter transect traced much of the CJP water, which was characterized by high temperature (Figure 2a) and low salinity (Figure 2b) extending from the estuary mouth to the midshelf. In the shallow inner shelf waters, temperature was high (29.2 °C), and the water column was well mixed. A thermocline existed around 20 m beyond the shallow inner shelf at Stations C4, C6, and C8 (Figure 2a). The cold and saline water mass below 30 m at

DOI: 10.1021/acs.est.5b06211
Environ. Sci. Technol. 2016, 50, 2255−2263

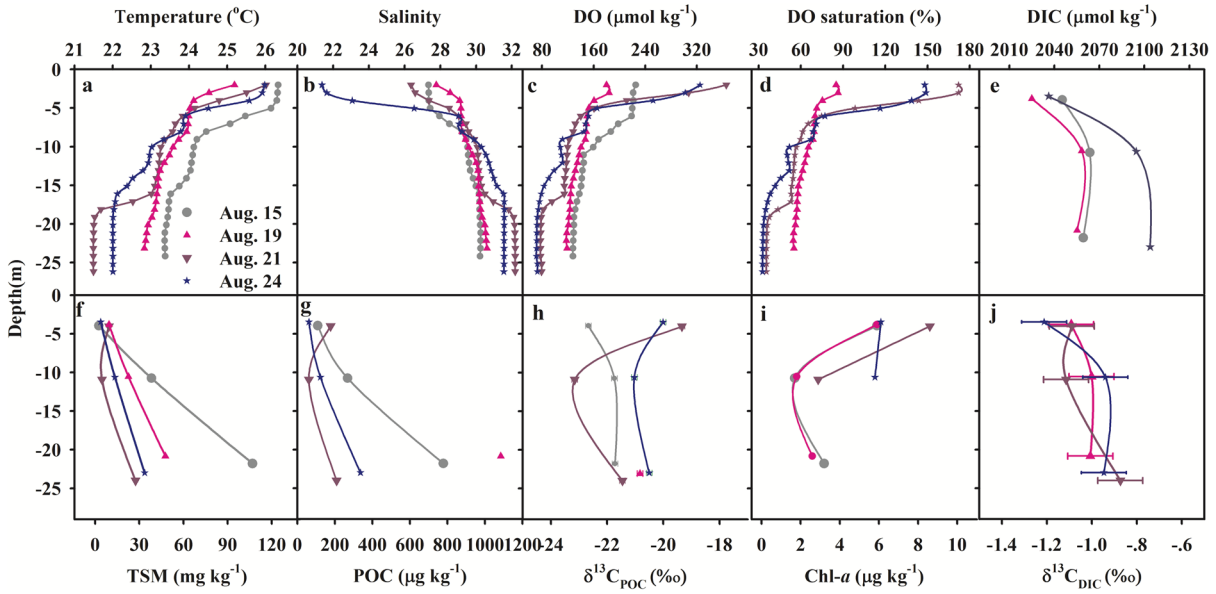

Figure 3. Profiles of (a) temperature, (b) salinity, (c) DO, (d) DO saturation, (e) DIC, (f) TSM, (g) POC, (h) $\delta^{13}C_{POC}$, (i) Chl-*a*, and (j) $\delta^{13}C_{DIC}$ and their evolution during repeated sampling at Station C4. Note that the temperature, salinity, DO, TSM, and Chl-*a* data presented in panels (a), (b), (f), and (i) are partially reported in Hsiao et al.[37]

Station C5 (Figure 2a and b), contained low DO (<100 μmol kg^{-1}) (Figure 2c) and high DIC (>2080 μmol kg^{-1}) (Figure 2d). The DO concentrations at other stations were greater than 143.8 μmol kg^{-1}. Both the CJP and surface water at Stations C6 and C8 were characterized by low DIC concentrations due to dilution by freshwater with low DIC (1840 μmol kg^{-1}) and strong photosynthesis reflected by the high Chl-*a* concentration (Figure 2f) in the offshore area.

The concentrations of POC (Figure 2e) and TSM (Figure 2g) were much higher nearshore than offshore at depths greater than 40 m. The TSM and POC concentrations at both Stations C1 and C2 reached 2050 mg kg^{-1} and 7610.1 μg kg^{-1}, while surface TSM at Station C5 was less than 4 mg kg^{-1}. Both TSM and POC in the bottom along the two transects were significantly higher than those in the surface water. Taking Station C4 (or A3) as an example, the bottom concentrations of TSM ranged from 47.7 to 106.9 mg kg^{-1} and POC ranged from 778 to 1084 μg kg^{-1} from August 15 to 19, 2011, which were much higher than those in the surrounding waters. Such enhancement should be primarily related to the resuspension of bottom sediments. At offshore stations such as C6, both surface Chl-*a* and POC concentrations were consistently high (Figure 2f and e).

The $\delta^{13}C_{POC}$ in the freshwater end-member (−24.4 ± 0.2‰) was much more depleted than in the offshore area (−21.0 ± 0.7‰) at $S > 30$ (Figure 2h). The $\delta^{13}C_{POC}$ above the thermocline (−19.2 ± 1.2‰) was generally heavier than below the thermocline (−21.5 ± 0.4‰) in Stations C6, C7, C8, T1, and T2. The $\delta^{13}C_{POC}$ generally increased from Station A1 to A7 with little difference between surface and bottom waters. The value of $\delta^{13}C_{DIC}$ (−8.5‰) nearshore reflected freshwater input and was more negative than the offshore value (from −1.2‰ to +0.8‰) at $S > 30$ (Figure 2i). The $\delta^{13}C_{DIC}$ in the offshore bottom water was about 0.2‰ more negative than that in the surface water.

An important context of our sampling campaign was the passing of Typhoon Muifa through the study area, which dramatically altered the hydrological condition and essentially eroded the stratification. The reestablishment of stratification and reinstatement of hypoxia can be exemplified by the evolution of DO as well as other hydrochemical parameters at Station C4, which was visited four times during the cruise (Figure 3).

At the beginning of our survey, the disturbance of the typhoon could be clearly seen from the vertical hydrological structure, that is, a relatively deeper thermocline or weak stratification, and the highest concentration of TSM in the bottom water. The stratification progressively became stronger during this 10 day period of our survey, and the bottom water TSM decreased sharply from 106.9 to 47.7 and then to 31.6 mg kg^{-1} toward the last visit, clearly demonstrating that the sediment resuspension driven by the typhoon diminished after about 2 weeks, as commonly observed in this area by other researchers.[49] The concentration of POC in the bottom water had a generally similar distribution and evolution pattern to that of the TSM, and the bottom POC was significantly higher than the surface value (Figure 3g).

Alongside the recovery of the water column stratification, the bottom water DO decreased monotonically from 127.9 μmol kg^{-1} (August 15), to 118.9 μmol kg^{-1} (August 19), to 77.6 μmol kg^{-1} (August 21), and to 71.3 μmol kg^{-1} (August 24) (Figure 2c), suggesting continuous DO consumption toward the reinstatement of hypoxia after the typhoon passage. This pattern of oxygen consumption was generally consistent with the bottom DIC release, an end product of aerobic respiration, which increased from 2059.3 μmol kg^{-1} (August 15) to 2103.8 μmol kg^{-1} (August 24) (Figure 3e). Also, the $\delta^{13}C_{DIC}$ value ranged from −1.2 to −0.9‰ (Figure 3j), and the value was more depleted in the surface water, resulting from the formation of a relatively fresher surface layer as observed by the low salinity near the surface.

As a result of the photosynthetic production of organic matter in the surface water (Figure 3g), surface DO increased from 221.4 on August 15 to 325.0 μmol kg^{-1} on August 24 (Figure 3c). The most intense photosynthesis took place on August 21 as evidenced by the highest surface DO (365.6 μmol kg^{-1}), Chl-*a* (8.6 μg kg^{-1}), and POC (177.0 μg kg^{-1}). The $\delta^{13}C_{POC}$ increased from −22.7 on August 15 to −19.7 ± 0.5‰ on August 21 and 24

DOI: 10.1021/acs.est.5b06211
Environ. Sci. Technol. 2016, 50, 2255−2263

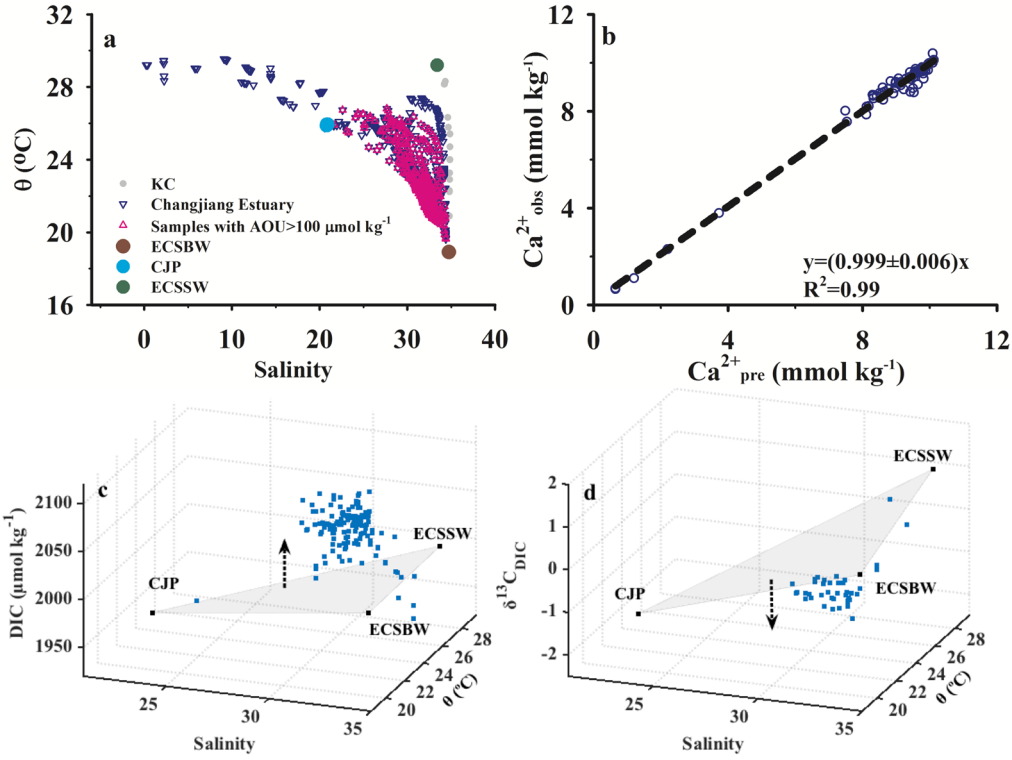

Figure 4. (a) Potential temperature (θ) (°C) vs salinity scheme in the East China Sea off the Changjiang Estuary (blue triangles) based on the data collected in the survey in August 2011. Also shown are the end-members for the East China Sea bottom water (ESCBW, brown dots), East China Sea surface water (ECSSW, green dots), and Changjiang plume water (CJP, cyan dots). (b) Relationship between the observed and model-predicted Ca^{2+} concentrations. (c) Three-dimensional scatter relationships between θ (°C), salinity, and DIC. (d) Three-dimensional scatter relationships between θ (°C), salinity, and $\delta^{13}C_{DIC}$. Shadowed patches in panels (c) and (d) represent the predicted conservative DIC and $\delta^{13}C_{DIC}$ controlled solely by physical mixing processes. Dark dashed arrows denote the difference of DIC or $\delta^{13}C_{DIC}$ concentrations between the predicted conservative values and field measurements.

Table 1. Summary of End-Member Values and Their Uncertainties Used in Our Three End-Member Mixing Model

water mass	salinity	temperature (°C)	DIC (μmol kg^{-1})	$\delta^{13}C_{DIC}$[a]	DIN (μmol kg^{-1})	DIP (μmol kg^{-1})	$Si(OH)_4$ (μmol kg^{-1})	Ca^{2+} (μmol kg^{-1})
CJP	21 ± 0.5	25.7 ± 0.5	1920 ± 10	−2.5 ± 0.1	59	1.03	52	6404
ECSSW	33.4 ± 0.1	29.2 ± 0.1	1991 ± 10	0.9 ± 0.1	0.1	0.02	2	9816
ECSBW	34.7 ± 0.1	18.9 ± 0.1	2018 ± 10	0.6 ± 0.1	3.69	0.55	22	10207

[a]The $\delta^{13}C_{DIC}$ value for ECSBW was collected from Leg 3, P03 section, at Station 376 (126.33°E, 26.74°N) at 200 m in *Field Activity of JAMSTEC toward International Repeat Hydrography and Carbon Program* (http://www.jamstec.go.jp/iorgc/ocorp/data/p03rev_2005/). The $\delta^{13}C_{DIC}$ value was 0.9‰ in the surface water of the outer plume area at $S > 32$ and −8.8‰ at $S < 0.2$ near the freshwater source from June to October in 2011. Our model adopted 0.9‰ as the ESCSW end-member ($S = 33.4$), while the $\delta^{13}C_{DIC}$ of CJP end-member ($S = 21$) was calculated based on isotope mass balance, which was −2.5‰.

in the surface water (Figure 3h). The $\delta^{13}C_{POC}$ value below 15 m fluctuated around 21.2 ± 0.6‰ during this 10 day period.

4. DISCUSSION

4.1. Selections of End-Members and Model Validation.

The potential temperature−salinity diagram illustrates a three end-member mixing scheme over the ECS shelf (Figure 4a), comprising the CJP water, ECS surface water (ECSSW), and ECS bottom water (ECSBW), similar to the observations in Chen and Wang.[50] According to Chen and Wang,[50] DIC was 2000 μmol kg^{-1} at $S = 33.4$, which can be regarded as the summer shelf surface water end-member or as the ECSSW end-member. The ECSBW originates from the Kuroshio water at a depth of ~200 m[51,52] with a DIC value of ~2018 μmol kg^{-1}.[53,54] The CJP water end-member was derived from the DIC−salinity conservative mixing curve, which was DIC = 5.716 × salinity + 1800. Here, we chose $S = 21$ as the CJP end-member because this end-member best represented the actual water mass mixing on the time scale of our field observation (Figure 4a). We note in the plume region at $S < 21$ that the mixing was actually dominated by two end-members mixing. This CJP end-member selection was decided also because there was practical difficulty in choosing the real freshwater end-member as the region under study was also affected by other freshwater input, such as that from the Huangpu Jiang, a highly urbanized tributary of Changjiang,[55] and from the Qiantang Jiang.[46] Nevertheless, even if we used a freshwater end-member, the outputs of the model only showed minor difference from those based on the CJP end-member at $S = 21$. The summary of the end-member values adopted in this study was given in Table 1.

On the basis of the model, we derived fractional contributions for any water parcel in the region to predict the values of biogeochemical parameters such as DIC and $\delta^{13}C_{DIC}$ (triangle

DOI: 10.1021/acs.est.5b06211
Environ. Sci. Technol. 2016, 50, 2255−2263

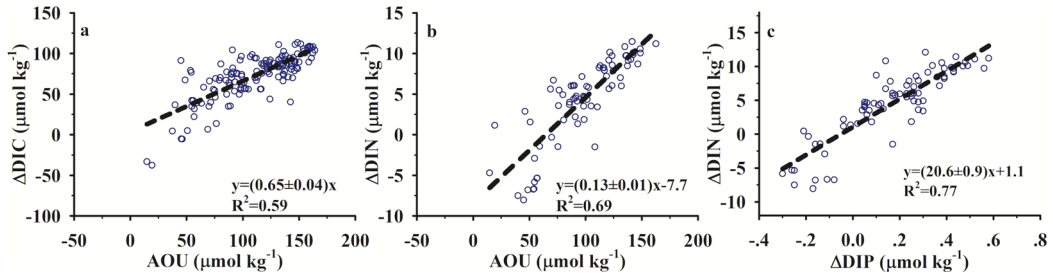

Figure 5. Plots of ΔDIC vs AOU (a), ΔDIN vs AOU (b), and ΔDIN vs ΔDIP (c) for all the data collected in the subsurface layer. Δ was the difference between the field-measured and model-predicted value of a biogeochemical parameter.

patch, Figure 4c and d) that were expected from conservative mixing using the end-member values given in Table 1. We used the concentration of Ca^{2+} as a conservative tracer to validate our model prediction. The agreement between Ca^{2+}_{obs} (field observed Ca^{2+} concentration) and Ca^{2+}_{pre} (model predicted Ca^{2+} concentration) in Figure 4b provided strong support for the validity of our model approach.

It is clear that the majority of observed DIC values in the subsurface were higher than the predicted values (Figure 4c), representing a DIC production due to OC remineralization, while the observed $\delta^{13}C_{DIC}$ values were lower than the predicted values (Figure 4d), resulting from lighter carbon accumulation. On the basis of the difference between the predicted and measured values of DIC and $\delta^{13}C_{DIC}$, the isotope of carbon that consumed DO could be calculated (see details in Section 4.2).

As shown in Figure 5a, ΔDIC has a clear positive correlation with apparent oxygen utilization (AOU), consistent with the fact that additional DIC is produced by organic matter remineralization via aerobic respiration. The slope of ΔDIC vs AOU in subsurface water is 0.65 ± 0.04, which is close to the classic Redfield stoichiometry (i.e., 106/138 = 0.77), and provides further evidence for the occurrence of aerobic respiration. It is interesting that the calculated ΔDIC and AOU ratio matches the Hedges version of the Redfield ratio (0.68) based on the mean composition of real marine organic matter.[56]

Additionally, the ΔDIN (biologically altered fraction of dissolved inorganic nitrogen) and AOU ratio (Figure 5b) is 0.13 ± 0.01, which is also close to the Redfield ratio (16/138 = 0.12). The model derived ΔDIN and ΔDIP (biologically altered fraction of dissolved inorganic phosphorus) ratio is 20.6 ± 0.9 (Figure 5c), which is higher than but within a reasonable range of the Redfield N/P = 16 ratio from respiratory processes. Taken together, the validation from field observations and intrinsic biogeochemical principles shows that our three end-member mixing model is suitable in the study area.

4.2. Isotopic Composition of the Oxygen Consumed OC. The mass balance of the DIC isotope composition is shown by eq 4.

$$\delta^{13}C_{DICobs} \times DIC_{obs} = \delta^{13}C_{DICpre} \times DIC_{pre} + \delta^{13}C_{DICbio} \times DIC_{bio} \quad (4)$$

where $\delta^{13}C_{DICobs}$ and DIC_{obs} are the field-observed values, while $\delta^{13}C_{DICpre}$ and DIC_{pre} are the model-predicted conservative values.

The isotopic composition of DIC_{bio} and $\delta^{13}C_{DICbio}$ should be identical to $\delta^{13}C_{OCx}$ of the OC that consumed oxygen and produced DIC_{bio}. Then, $\delta^{13}C_{OCx}$ can be derived based on the mass balance equations of both DIC and isotopic composition (eq 5).

$$\delta^{13}C_{OCx} = \frac{\delta^{13}C_{DICobs} \times DIC_{obs} - \delta^{13}C_{DICpre} \times DIC_{pre}}{DIC_{obs} - DIC_{pre}} \quad (5)$$

eq 5 can be rearranged into eq 6,

$$\Delta(\delta^{13}C_{DIC} \times DIC) = \delta^{13}C_{OCx} \times \Delta DIC \quad (6)$$

We plotted $\Delta(\delta^{13}C_{OCx} \times DIC)$ versus ΔDIC in Figure 6. The slope of the linear regression represents $\delta^{13}C_{OCx}$ or $\delta^{13}C_{DICbio}$,

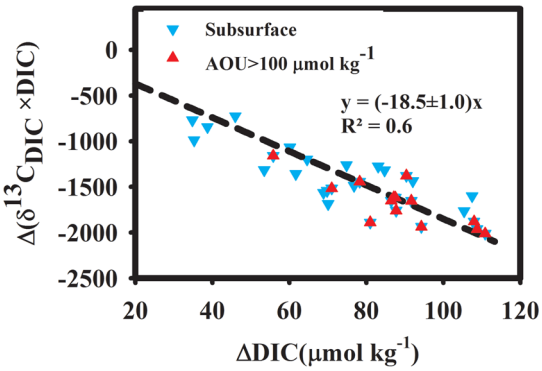

Figure 6. Plot of $\Delta(\delta^{13}C_{DIC} \times DIC)$ vs ΔDIC for samples collected in the subsurface (below 5 m). Note that red triangles are the samples with AOU > 100 μmol kg^{-1}. Δ denotes the difference between the model-predicted and the field-measured values.

which equals −18.5 ± 1.0‰. The $\delta^{13}C_{POC}$ at Station C1 (S = 0.2) averaged −24.4 ± 0.2‰ (Figure 2h), reflecting the terrestrial origin. Previous studies show that the $\delta^{13}C$ for the riverine POC in the Changjiang ranges from −26.6 to −24.9‰.[57,58] Similarly, Zhu et al.[59] report an average $\delta^{13}C$ value of −24.3 ± 0.3‰, reflecting multiple allochthonous inputs, including C4 and C3 plant debris.[60,61] The surface layer data at all stations with high salinity and high Chl-*a* had an average $\delta^{13}C_{POC}$ of −19.1 ± 0.5‰, and the average $\delta^{13}C_{POC}$ value in the surface water of Stations T1 and T2 was −18.5 ± 0.3‰, where a bloom occurred with high Chl-*a* value ranging 16.2−93.4 μg kg^{-1} as shown in Tseng et al.[46] So it is reasonable to assign −18.5 ± 0.3‰ as the $\delta^{13}C$ value of OC_{mar} in the ECS. A similar marine POC end-member of −19‰ was adopted for this area in other research.[62] Thus, the $\delta^{13}C$ of the remineralized organic matter we derived (−18.5 ± 1.0‰) was reasonably close, within the uncertainty, to the OC_{mar} isotopic signal (−18.5 ± 0.3‰). This predominance of OC_{mar} remineralization in the hypoxic system likely implied that OC_{terr} in the coastal ocean water column was less dominant or less reactive.

This study did not account for the contribution of DOC to oxygen consumption. This notion was based on the fact that

DOI: 10.1021/acs.est.5b06211
Environ. Sci. Technol. 2016, 50, 2255−2263

DOC was almost conservative in the subsurface water in our study area (data not shown), suggesting that the oxidation of DOC, if any, would be minor. According to other studies, the $\delta^{13}C_{DOC}$ values in terrestrial sources (−25 to −32‰), are also more depleted than the marine source (−20 to −23‰).[63−65] For example, Guo et al.[64] found a $\delta^{13}C_{DOC}$ increase from −25.2‰ at the Mississippi River freshwater to −21.9‰ at an offshore station, while there is a $\delta^{13}C_{POC}$ increase from −25.3 to −20.6‰ in the northern Gulf of Mexico.[65] The $\delta^{13}C_{DOC}$ is not generally significantly different from $\delta^{13}C_{POC}$ in different systems.[66−68] Even if some DOC was remineralized in the Changjiang estuary, it would only affect the carbon species, rather than the relative contribution of OC_{mar} or OC_{terr} to the DO consumption. We must point out that our observation was conducted 10 days after a typhoon passage, which clearly stimulated significant sediment resuspension, and thus, both particulate organic material that sunk out of the surface and resuspended from sediments would consume oxygen in the subsurface waters, which could not be distinguished in this study because both of the isotopic signals would have been reflected in that of the decomposition product, DIC, and the derived $\delta^{13}C$ of the decomposed OC. However, the ultimate sources of organic material that consumed oxygen would be from the marine biomass productivity based on the derived $\delta^{13}C$ of the decomposed OC. Also, our method illustrated here examined the respirational end product DIC to trace back the decomposed carbon, so it has applicability to other environmental settings and conditions.

Taken together, the remineralization of OC_{mar} overwhelmingly contributed to DO consumption in the stratified subsurface waters in the ECS off the Changjiang estuary. This study has significant implications for decision-making that seeks to mitigate and/or remediate hypoxic ecosystems. Reduction of nutrient runoff, thus controlling eutrophication, is indeed the key. The nutrient loading in many large river systems actually shows a substantial increase since the early 20th century, while terrestrial OC discharge remains relatively unchanged[69] or even declined due to damming.[70] The continuing expansion of coastal hypoxia across the globe is thus not surprising due to the increased nutrient flux from adjacent watersheds. Modeling studies also suggest that future climate and land-use changes will result in more extensive eutrophication and hypoxia in most large-river-impacted ocean margins, increasing the urgency for remediation measures and action in coastal ecosystems.[71] This is particularly true for China, where nutrient emissions have been growing very strongly since the early 1980s, while the United States and Europe stabilized their fertilizer usage in the 1980s or early 1990s.[33]

AUTHOR INFORMATION

Corresponding Author

*E-mail: mdai@xmu.edu.cn. Phone: 86-592-2182132. Fax: 86-592-218-4101.

Notes

The authors declare no competing financial interest.

ACKNOWLEDGMENTS

This research was funded by the Ocean Public Welfare Scientific Research Project, State Oceanic Administration of China through Grant #2015418003-3 and #200905012-6 and NSF-China through Grants #41121091 and #4102164005. Hongjie Wang was partially supported by the Gulf of Mexico Research Initiative (RFP-II). We thank Jianping Cao, Xijie Yin, and Hailong Zhang for their assistance with stable isotope analyses. Xu Dong, Yan Li, Liguo Guo, Weidong Zhai, Huade Zhao, Qian Li, Kuanbo Zhou, Zhimian Cao, Chuanjun Du, Xinping Hu, and Nancy Rabalais provided comments on the earlier versions of the paper. Comments and suggestions from three anonymous reviewers and the associate editor, Miriam Diamond, have greatly improved the quality of the paper. John Hodgkiss is thanked for his editorial help with English. Data are available upon request to mel.xmu.edu.cn.

REFERENCES

(1) Conley, D. J.; Carstensen, J.; Aigars, J.; Axe, P.; Bonsdorff, E.; Eremina, T.; Haahti, B.-M.; Humborg, C.; Jonsson, P.; Kotta, J. Hypoxia Is Increasing in the Coastal Zone of the Baltic Sea. *Environ. Sci. Technol.* **2011**, *45*, 6777−6783.

(2) Diaz, R. J. Overview of hypoxia around the world. *J. Environ. Qual.* **2001**, *30*, 275−281.

(3) Diaz, R. J.; Rosenberg, R. Spreading dead zones and consequences for marine ecosystems. *Science* **2008**, *321*, 926−929.

(4) Levin, L.; Ekau, W.; Gooday, A.; Jorissen, F.; Middelburg, J.; Naqvi, S.; Neira, C.; Rabalais, N.; Zhang, J. Effects of natural and human-induced hypoxia on coastal benthos. *Biogeosciences* **2009**, *6*, 2063−2098.

(5) Zhang, J.; Gilbert, D.; Gooday, A.; Levin, L.; Naqvi, S.; Middelburg, J.; Scranton, M.; Ekau, W.; Pena, A.; Dewitte, B.; et al. Natural and human-induced hypoxia and consequences for coastal areas: synthesis and future development. *Biogeosciences* **2010**, *7*, 1443−1467.

(6) Middelburg, J. J.; Levin, L. A. Coastal hypoxia and sediment biogeochemistry. *Biogeosciences* **2009**, *6*, 1273−1293.

(7) Cai, W. J.; Hu, X.; Huang, W.-J.; Murrell, M. C.; Lehrter, J. C.; Lohrenz, S. E.; Chou, W.-C.; Zhai, W.; Hollibaugh, J. T.; Wang, Y.; et al. Acidification of subsurface coastal waters enhanced by eutrophication. *Nat. Geosci.* **2011**, *4*, 766−770.

(8) Rabouille, C.; Conley, D. J.; Dai, M. H.; Cai, W. J.; Chen, C. T. A.; Lansard, B.; Green, R.; Yin, K.; Harrison, P. J.; Dagg, M.; McKee, B. Comparison of hypoxia among four river-dominated ocean margins: The Changjiang (Yangtze), Mississippi, Pearl, and Rhône rivers. *Cont. Shelf Res.* **2008**, *28*, 1527−1537.

(9) Carstensen, J.; Andersen, J. H.; Gustafsson, B. G.; Conley, D. J. Deoxygenation of the Baltic Sea during the last century. *Proc. Natl. Acad. Sci. U. S. A.* **2014**, *111*, 5628−5633.

(10) Chen, C.-C.; Gong, G.-C.; Shiah, F.-K. Hypoxia in the East China Sea: One of the largest coastal low-oxygen areas in the world. *Mar. Environ. Res.* **2007**, *64*, 399−408.

(11) Kemp, W.; Testa, J.; Conley, D.; Gilbert, D.; Hagy, J. Temporal responses of coastal hypoxia to nutrient loading and physical controls. *Biogeosciences* **2009**, *6*, 2985−3008.

(12) Rabalais, N. N.; Turner, R. E.; Wiseman, W. J. Gulf of Mexico Hypoxia, A.K.A. "The Dead Zone. *Annu. Rev. Ecol. Syst.* **2002**, *33*, 235−263.

(13) Fry, B.; Justić, D.; Riekenberg, P.; Swenson, E. M.; Turner, R. E.; Wang, L.; Pride, L.; Rabalais, N. N.; Kurtz, J. C.; Lehrter, J. C.; et al. Carbon Dynamics on the Louisiana Continental Shelf and Cross-Shelf Feeding of Hypoxia. *Estuaries Coasts* **2015**, *38*, 703−721.

(14) Murphy, R.; Kemp, W. M.; Ball, W. Long-Term Trends in Chesapeake Bay Seasonal Hypoxia, Stratification, and Nutrient Loading. *Estuaries Coasts* **2011**, *34*, 1293−1309.

(15) Rabalais, N. N.; Cai, W.-J.; Carstensen, J.; Conley, D. J.; Fry, B.; Hu, X.; Quinones-Rivera, Z.; Rosenberg, R.; Slomp, C. P.; Turner, R. E.; et al. Eutrophication-Driven Deoxygenation in the Coastal Ocean. *Oceanography* **2014**, *27*, 172−183.

(16) Thibodeau, B.; de Vernal, A.; Mucci, A. Recent eutrophication and consequent hypoxia in the bottom waters of the Lower St. Lawrence Estuary: Micropaleontological and geochemical evidence. *Mar. Geol.* **2006**, *231*, 37−50.

(17) Zhu, Z.-Y.; Zhang, J.; Wu, Y.; Zhang, Y.-Y.; Lin, J.; Liu, S.-M. Hypoxia off the Changjiang (Yangtze River) Estuary: oxygen depletion and organic matter decomposition. *Mar. Chem.* **2011**, *125*, 108−116.

DOI: 10.1021/acs.est.5b06211
Environ. Sci. Technol. 2016, 50, 2255−2263

(18) Bianchi, T. S.; DiMarco, S. F.; Cowan, J. H., Jr; Hetland, R. D.; Chapman, P.; Day, J. W.; Allison, M. A. The science of hypoxia in the northern Gulf of Mexico: A review. *Sci. Total Environ.* **2010**, *408*, 1471−1484.
(19) Bianchi, T. S.; Wysocki, L. A.; Schreiner, K. M.; Filley, T. R.; Corbett, D. R.; Kolker, A. S. Sources of terrestrial organic carbon in the Mississippi plume region: evidence for the importance of coastal marsh inputs. *Aquat. Geochem.* **2011**, *17*, 431−456.
(20) Swarzenski, P. W.; Campbell, P. L.; Osterman, L. E.; Poore, R. Z. A 1000-year sediment record of recurring hypoxia off the Mississippi River: The potential role of terrestrially-derived organic matter inputs. *Mar. Chem.* **2008**, *109*, 130−142.
(21) Dagg, M.; Ammerman, J.; Amon, R. W.; Gardner, W.; Green, R.; Lohrenz, S. A review of water column processes influencing hypoxia in the northern Gulf of Mexico. *Estuaries Coasts* **2007**, *30*, 735−752.
(22) Green, R.; Bianchi, T.; Dagg, M.; Walker, N.; Breed, G. An organic carbon budget for the Mississippi River turbidity plume and plume contributions to air-sea CO_2 fluxes and bottom water hypoxia. *Estuaries Coasts* **2006**, *29*, 579−597.
(23) Rabalais, N. N.; Turner, R. E.; Sen Gupta, B. K.; Boesch, D. F.; Chapman, P.; Murrell, M. C. Hypoxia in the northern Gulf of Mexico: Does the science support the plan to reduce, mitigate, and control hypoxia? *Estuaries Coasts* **2007**, *30*, 753−772.
(24) Turner, R. E.; Rabalais, N. N.; Justic, D. Predicting summer hypoxia in the northern Gulf of Mexico: Riverine N, P, and Si loading. *Mar. Pollut. Bull.* **2006**, *52*, 139−148.
(25) Li, D.; Zhang, J.; Huang, D.; Wu, Y.; Liang, J. Oxygen depletion off the Changjiang (Yangtze River) estuary. *Sci. China, Ser. D: Earth Sci.* **2002**, *45*, 1137−1146.
(26) Li, X.; Bianchi, T. S.; Yang, Z.; Osterman, L. E.; Allison, M. A.; DiMarco, S. F.; Yang, G. Historical trends of hypoxia in Changjiang River estuary: Applications of chemical biomarkers and microfossils. *J. Mar. Syst.* **2011**, *86*, 57−68.
(27) Wang, B.; Wei, Q.; Chen, J.; Xie, L. Annual cycle of hypoxia off the Changjiang (Yangtze River) Estuary. *Mar. Environ. Res.* **2012**, *77*, 1−5.
(28) Milliman, J. D.; Meade, R. H. World-Wide Delivery of River Sediment to the Oceans. *J. Geol.* **1983**, *91*, 1−21.
(29) Liu, S.; Hong, G.-H.; Zhang, J.; Ye, X.; Jiang, X. Nutrient budgets for large Chinese estuaries. *Biogeosciences* **2009**, *6*, 2245−2263.
(30) Wang, X.; Ma, H.; Li, R.; Song, Z.; Wu, J. Seasonal fluxes and source variation of organic carbon transported by two major Chinese Rivers: The Yellow River and Changjiang (Yangtze) River. *Global. Biogeochem. Cy.* **2012**, DOI: 10.1029/2011GB004130.
(31) Zhou, M.-j.; Shen, Z.-l.; Yu, R.-c. Responses of a coastal phytoplankton community to increased nutrient input from the Changjiang (Yangtze) River. *Cont. Shelf Res.* **2008**, *28*, 1483−1489.
(32) Li, M.; Xu, K.; Watanabe, M.; Chen, Z. Long-term variations in dissolved silicate, nitrogen, and phosphorus flux from the Yangtze River into the East China Sea and impacts on estuarine ecosystem. *Estuarine, Coastal Shelf Sci.* **2007**, *71*, 3−12.
(33) Liu, X.; Zhang, Y.; Han, W.; Tang, A.; Shen, J.; Cui, Z.; Vitousek, P.; Erisman, J. W.; Goulding, K.; Christie, P.; et al. Enhanced nitrogen deposition over China. *Nature* **2013**, *494*, 459−462.
(34) Wang, B. Hydromorphological mechanisms leading to hypoxia off the Changjiang estuary. *Mar. Environ. Res.* **2009**, *67*, 53−58.
(35) Wei, H.; He, Y.; Li, Q.; Liu, Z.; Wang, H. Summer hypoxia adjacent to the Changjiang Estuary. *J. Marine Syst.* **2007**, *67*, 292−303.
(36) Chen, C.; Zhu, J.; Beardsley, R. C.; Franks, P. J. S. Physical-biological sources for dense algal blooms near the Changjiang River. *Geophys. Res. Lett.* **2003**, DOI: 10.1029/2002GL016391.
(37) Hsiao, S.-Y.; Hsu, T.-C.; Liu, J.-w.; Xie, X.; Zhang, Y.; Lin, J.; Wang, H.; Yang, J.-Y.; Hsu, S.-C.; Dai, M.; Kao, S.-J. Nitrification and its oxygen consumption along the turbid Chang Jiang River plume. *Biogeosciences* **2014**, *11*, 2083−2098.
(38) Chen, Z.; Li, J.; Shen, H.; Zhanghua, W. Yangtze River of China: historical analysis of discharge variability and sediment flux. *Geomorphology* **2001**, *41*, 77−91.
(39) Jiang, T.; Su, B.; Hartmann, H. Temporal and spatial trends of precipitation and river flow in the Yangtze River Basin, 1961−2000. *Geomorphology* **2007**, *85*, 143−154.
(40) Dai, M.; Guo, X.; Zhai, W.; Yuan, L.; Wang, B.; Wang, L.; Cai, P.; Tang, T.; Cai, W.-J. Oxygen depletion in the upper reach of the Pearl River estuary during a winter drought. *Mar. Chem.* **2006**, *102*, 159−169.
(41) Cai, W.-J.; Dai, M.; Wang, Y.; Zhai, W.; Huang, T.; Chen, S.; Zhang, F.; Chen, Z.; Wang, Z. The biogeochemistry of inorganic carbon and nutrients in the Pearl River estuary and the adjacent Northern South China Sea. *Cont. Shelf Res.* **2004**, *24*, 1301−1319.
(42) Cao, Z.; Dai, M. Shallow-depth $CaCO_3$ dissolution: Evidence from excess calcium in the South China Sea and its export to the Pacific Ocean. *Global Biogeochem. Cy.* **2011**, DOI: 10.1029/2009GB003690.
(43) Chen, B.; Liu, H.; Landry, M. R.; Dai, M.; Huang, B.; Sun, J. Close coupling between phytoplankton growth and microzooplankton grazing in the western South China Sea. *Limnol. Oceanogr.* **2009**, *54*, 1084−1097.
(44) Kao, S. J.; Terence Yang, J. Y.; Liu, K. K.; Dai, M.; Chou, W. C.; Lin, H. L.; Ren, H. Isotope constraints on particulate nitrogen source and dynamics in the upper water column of the oligotrophic South China Sea. *Global Biogeochem. Cy.* **2012**, DOI: 10.1029/2011GB004091.
(45) Xing, L.; Zhang, H.; Yuan, Z.; Sun, Y.; Zhao, M. Terrestrial and marine biomarker estimates of organic matter sources and distributions in surface sediments from the East China Sea shelf. *Cont. Shelf Res.* **2011**, *31*, 1106−1115.
(46) Tseng, Y.-F.; Lin, J.; Dai, M.; Kao, S.-J. Joint effect of freshwater plume and coastal upwelling on phytoplankton growth off the Changjiang River. *Biogeosciences* **2014**, *11*, 409−423.
(47) Han, A.; Dai, M.; Kao, S.-J.; Gan, J.; Li, Q.; Wang, L.; Zhai, W.; Wang, L. Nutrient dynamics and biological consumption in a large continental shelf system under the influence of both a river plume and coastal upwelling. *Limnol. Oceanogr.* **2012**, *57*, 486−502.
(48) Cao, Z.; Dai, M.; Zheng, N.; Wang, D.; Li, Q.; Zhai, W.; Meng, F.; Gan, J. Dynamics of the carbonate system in a large continental shelf system under the influence of both a river plume and coastal upwelling. *J. Geophys. Res.* **2011**, *116*, na DOI: 10.1029/2010JG001596.
(49) Bian, C.; Jiang, W.; Song, D. Terrigenous transportation to the Okinawa Trough and the influence of typhoons on suspended sediment concentration. *Cont. Shelf Res.* **2010**, *30*, 1189−1199.
(50) Chen, C. T. A.; Wang, S. L. Carbon, alkalinity and nutrient budgets on the East China Sea continental shelf. *J. Geophys. Res.-Oceans* **1999**, *104* (C9), 20675−20686.
(51) Yang, D.; Yin, B.; Liu, Z.; Bai, T.; Qi, J.; Chen, H. Numerical study on the pattern and origins of Kuroshio branches in the bottom water of southern East China Sea in summer. *J. Geophys. Res.* **2012**, *117*, na DOI: 10.1029/2011JC007528.
(52) Yang, D.; Yin, B.; Liu, Z.; Feng, X. Numerical study of the ocean circulation on the East China Sea shelf and a Kuroshio bottom branch northeast of Taiwan in summer. *J. Geophys. Res.* **2011**, *116*, na DOI: 10.1029/2010JC006777.
(53) Sheu, D. D.; Chou, W.-C.; Chen, C. T. A.; Wei, C.-L.; Hsieh, H.-L.; Hou, W.-P.; Dai, M. Riding over the Kuroshio from the South to the East China Sea: Mixing and transport of DIC. *Geophys. Res. Lett.* **2009**, DOI: 10.1029/2008GL037017.
(54) Chou, W. C.; Sheu, D. D.; Chen, C.; Wen, L. S.; Yang, Y.; Wei, C. L. Transport of the South China Sea subsurface water outflow and its influence on carbon chemistry of Kuroshio waters off southeastern Taiwan. *J. Geophys. Res.* **2007**, *112*, na DOI: 10.1029/2007JC004087.
(55) Zhai, W.; Dai, M.; Guo, X. Carbonate system and CO_2 degassing fluxes in the inner estuary of Changjiang (Yangtze) River, China. *Mar. Chem.* **2007**, *107*, 342−356.
(56) Hedges, J.; Baldock, J. A.; Gélinas, Y.; Lee, C.; Peterson, M.; Wakeham, S. The biochemical and elemental compositions of marine plankton: A NMR perspective. *Mar. Chem.* **2002**, *78*, 47−63.
(57) Wu, Y.; Zhang, J.; Liu, S. M.; Zhang, Z. F.; Yao, Q. Z.; Hong, G. H.; Cooper, L. Sources and distribution of carbon within the Yangtze River system. *Estuarine, Coastal Shelf Sci.* **2007**, *71*, 13−25.

DOI: 10.1021/acs.est.5b06211
Environ. Sci. Technol. 2016, 50, 2255−2263

(58) Zhang, J.; Wu, Y.; Jennerjahn, T.; Ittekkot, V.; He, Q. Distribution of organic matter in the Changjiang (Yangtze River) Estuary and their stable carbon and nitrogen isotopic ratios: Implications for source discrimination and sedimentary dynamics. *Mar. Chem.* **2007**, *106*, 111−126.
(59) Zhu, C.; Wagner, T.; Pan, J. M.; Pancost, R. D. Multiple sources and extensive degradation of terrestrial sedimentary organic matter across an energetic, wide continental shelf. *Geochem., Geophys., Geosyst.* **2011**, *12*, Q08011.
(60) Farquhar, G. D.; Ehleringer, J. R.; Hubick, K. T. Carbon isotope discrimination and photosynthesis. *Annu. Rev. Plant Physiol. Plant Mol. Biol.* **1989**, *40*, 503−537.
(61) Hobbie, E. A.; Werner, R. A. Intramolecular, compound-specific, and bulk carbon isotope patterns in C3 and C4 plants: a review and synthesis. *New Phytol.* **2004**, *161*, 371−385.
(62) Wu, Y.; Zhang, J.; Li, D. J.; Wei, H.; Lu, R. X. Isotope variability of particulate organic matter at the PN section in the East China Sea. *Biogeochemistry* **2003**, *65*, 31−49.
(63) Benner, R.; Biddanda, B.; Black, B.; McCarthy, M. Abundance, size distribution, and stable carbon and nitrogen isotopic compositions of marine organic matter isolated by tangential-flow ultrafiltration. *Mar. Chem.* **1997**, *57*, 243−263.
(64) Guo, L.; White, D. M.; Xu, C.; Santschi, P. H. Chemical and isotopic composition of high-molecular-weight dissolved organic matter from the Mississippi River plume. *Mar. Chem.* **2009**, *114*, 63−71.
(65) Wang, X. C.; Chen, R. F.; Gardner, G. B. Sources and transport of dissolved and particulate organic carbon in the Mississippi River estuary and adjacent coastal waters of the northern Gulf of Mexico. *Mar. Chem.* **2004**, *89*, 241−256.
(66) Raymond, P. A.; Bauer, J. E. Use of ^{14}C and ^{13}C natural abundances for evaluating riverine, estuarine, and coastal DOC and POC sources and cycling: a review and synthesis. *Org. Geochem.* **2001**, *32*, 469−485.
(67) Raymond, P. A.; Bauer, J. E.; Caraco, N. F.; Cole, J. J.; Longworth, B.; Petsch, S. T. Controls on the variability of organic matter and dissolved inorganic carbon ages in northeast US rivers. *Mar. Chem.* **2004**, *92*, 353−366.
(68) Deutsch, B.; Alling, V.; Humborg, C.; Korth, F.; Mörth, C. Tracing inputs of terrestrial high molecular weight dissolved organic matter within the Baltic Sea ecosystem. *Biogeosciences* **2012**, *9*, 4465−4475.
(69) Dai, M.; Yin, Z.; Meng, F.; Liu, Q.; Cai, W.-J. Spatial distribution of riverine DOC inputs to the ocean: an updated global synthesis. *Curr. Opin. Environ. Sustain.* **2012**, *4*, 170−178.
(70) Bianchi, T. S.; Allison, M. A. Large-river delta-front estuaries as natural "recorders" of global environmental change. *Proc. Natl. Acad. Sci. U. S. A.* **2009**, *106*, 8085−8092.
(71) Rabalais, N. N.; Turner, R. E.; Díaz, R. J.; Justić, D. Global change and eutrophication of coastal waters. *ICES J. Mar. Sci.* **2009**, *66*, 1528−1537.

DOI: 10.1021/acs.est.5b06211
Environ. Sci. Technol. 2016, 50, 2255−2263